IMPROVING EXPLANATIONS OF IMAGE CLASSIFICATION WITH ENSEMBLES OF LEARNERS

Aadil Ahamed[1], Kamran Alipour[1], Sateesh Kumar[1],
Severine Soltani[2] and Michael Pazzani[3]

[1]Department of Computer Science and Engineering,
University of California, San Diego,La Jolla, CA, USA
[2]Department of Bioengineering,
University of California, San Diego, La Jolla, CA, USA
[3]Information Sciences Institute, Marina Del Rey, CA, USA

ABSTRACT

In explainable AI (XAI) for deep learning, saliency maps, heatmaps, or attention maps are commonly used to identify important regions for the classification of images of explanations. Recent research has shown that many common XAI methods do not accurately identify the regions that human experts consider important. We propose averaging explanations from ensembles of learners to increase the accuracy of explanations. Our technique is general and can be used with multiple deep learning architectures and multiple XAI algorithms. We show that this method decreases the difference between regions of interest of XAI algorithms and those identified by human experts. Furthermore, we show that human experts prefer the explanations produced by ensembles to those of individual networks.

KEYWORDS

Neural Networks, Machine Learning, Explainable AI, Image Classification, Computer Vision.

1. INTRODUCTION

A variety of eXplainable Artificial Intelligence (XAI) methods have emerged for explaining image classification [15, 17] to developers or end-users [16, 6]. These approaches typically locate and highlight regions of the image that are important to the classification decision. Recently, several papers have called into question the ability of existing XAI methods to accurately identify regions that are meaningful to human experts such as radiologists, dermatologists, neurologists, oncologists, ophthalmologists, or even bird watchers [30, 8, 33, 22]. For example, [2] discusses the substantial differences between the regions on an x-ray that radiologists find important and those found by XAI algorithms.

We explore the use of ensemble learning [9] of neural networks to increase the accuracy of identifying regions of interest for any XAI algorithm by combining explanations from multiple neural networks. To illustrate, Figure 1(a-d) shows the heatmap of four neural networks trained on the same image data starting with different initial random weights. The task was to determine the wing pattern (e.g., striped, solid, spotted, wingbar). Figure 1(e) shows the heatmap produced by averaging the heatmaps of 11 networks. Of course, a disadvantage of our approach is that it requires more computation to create an ensemble than a single network. This linear increase in

David C. Wyld et al. (Eds): AI, AIMLNET, BIOS, BINLP, CSTY, MaVaS, SIGI - 2022
pp. 01-16, 2022. CS & IT - CSCP 2022 DOI: 10.5121/csit.2022.121801

computation can be mitigated by coarse-grained parallel training of N networks.

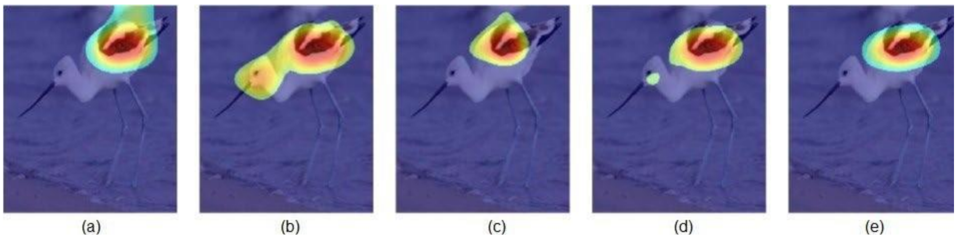

Figure 1. Saliency maps from an ensemble of classifiers. (a-d) are individual networks trained to identify the wing pattern. (e) is an average of 11 networks.

There are multiple purposes for XAI. One is to inform developers and perhaps validators how the deep learning system is working. Figure 2a shows an example heatmap produced by XAI algorithms to illustrate how the underlying deep learner operates. A second use which becomes important as applications of deep learning are deployed is to describe to end users the location of important diagnostic features. For example, Figure 2b shows an image from a dermatology journal [21] with three regions identified and labeled with *"milky pink structureless areas centrally* ***(*),*** *white streaks (^) and atypical pigment network (arrows)."* In this case, it is important for a deep learner and XAI system to not only get the correct diagnosis but also to correctly identify where the white streaks are.

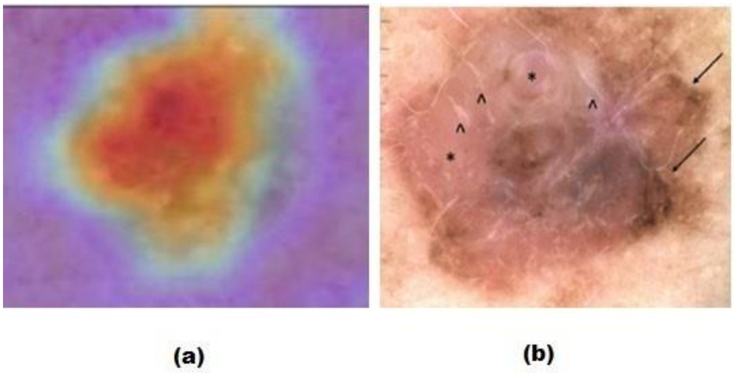

Figure 2. (a) Heatmap for explaining melanoma classification. (b) Image from journal explainingmelanoma diagnosis.

In the remainder of this paper, we first describe the methods we use to generate an ensemble of networks. Second, we discuss our evaluation methods which compare the regions of interest of an XAI algorithm to the regions of interest identified by people. Third, we describe the databases used in evaluation. Fourth, we describe the results using ensembles starting with different random weights on several problems. Fifth, we generalize our results by using two additional approaches to generating an ensemble of networks. Furthermore, we show the impact of varying the number of networks in the ensemble. Finally, we present results from an experiment with experienced bird watchers that show that they prefer the explanations from ensembles to those of individual networks.

2. PRIOR WORK

There are two main approaches in XAI to identify regions of interest in deep learning for image classification:

a. Model agnostic methods, such as LIME [23], manipulate inputs (e.g., pixels, regions or more commonly superpixels) and measure how changes in input affect output. If an input perturbation has no effect, it is not relevant to findings. If a change has a major impact (e.g., changing the classification from pneumonia to normal), then the region is important to the classification. Shapley Additive Explanations (SHAP) [20] uses a game-theoretic measure to assign each feature or region an importance value for a particular prediction.

b. Other methods examine the activations or weights of the deep network to find regionsof importance. Grad-CAM [26], Integrated Gradients [31], Saliency [28], GradientShap [19], and Layerwise Relevance Propagation LRP [25] are examples of such methods.

Ensemble learning has long been used to reduce the error of machine learning methods, including neural networks [11]. This error reduction is due to reduction in variance in the learned models [10]. Ensemble learning reduces errors most when the errors of the individual models are not highly correlated [1, 18]. Recent work [32] has shown that XAI methods for deep learners trained under slightly different circumstances produce explanations that are not highly correlated. The variability occurs due to the initial random parameter selection or the random order of training examples. This suggests that we can reduce the error of an explanation by combining explanations from an ensemble of networks.

Reiger [24] proposed combining different XAI methods such as Grad-CAM and LRP since each method has their own strengths and weakness and found this increased the stability of the XAI output. This does not use an ensemble of learners and cannot increase the accuracy of the classifications.

In learning from tabular data, ensembles have been shown to improve accuracy at the expense of interpretability. In contrast, our goal with image data is to both improve classification accuracy and the explanation.

3. METHODS

3.1. Generating Ensemble Explanations

For this paper, we use two common image classifiers: VGG16 [29] and ResNet [14]. We consider three methods of generating a diverse ensemble of classifiers.

1. **Different Random Weights**. We start with ***N*** identical base networks and then initialize each of the N classification heads with different random weights and present the same training data to each network. The idea here is that based on the initial conditions, the network will find a slightly different solution [3]. We evaluate whether on average the ensemble produces a better explanation than the members of the ensemble.

2. **Leave Out One Bucket.** We divide the training data into ***N*** buckets and train the ***N*** identical architectures on ***N-1*** buckets [13]. We evaluate whether the ensemble producesa better explanation than a single network trained on all the data.

3. **Bootstrap Aggregation.** We use bagging [4] which creates ***N*** training sets by sampling with replacement from the original training data. This leaves out some of the original training data and places additional weight on other examples by replicating them. We evaluate whether the ensemble produces a better explanation than network trained on all the data. The motivation of the latter two methods is that slightly different training data will

result in slightly different solutions that may be averaged. Even if each of the individual networks is less accurate than training on all the data, the consensus on the ensemble often exceeds the classification accuracy of a single network on all data. We anticipate this will hold with the accuracy of the explanation as well.

Once the models are trained, we generate an ensemble explanation by averaging the relevance score for each pixel (i, j) in the input image as shown in Eq. 1.

$$score_{ens}(i,j) = \frac{1}{n}\sum_{k=1}^{n} score_k(i,j) \tag{1}$$

3.2. Metrics

We consider three measures of explanation accuracy: Intersection over Union (IoU), correlation, and the center of mass distance. In all cases, the ground truth region is collected from human annotators. It is worth stressing that this region information is used only in evaluation, not in training.

1. **Intersection over Union** For IoU, we binarize the generated explanation by normalizing it between 0 and 1 (or [-1,1] for some XAI algorithms) and setting a threshold to find regions of interest. The IoU score is obtained by computing the intersection between the explanation and ground truth mask and then dividing it by their union. We use a default threshold of 0.3 in this work. Figure 3 illustrates how we compute the IoU score for a single image. The IoU metric allows us to compare how well an XAI algorithm identifies region of interest found by human annotators. A higher value shows more agreement between the algorithm and the annotator.

2. **Correlation** To quantify the similarities between explanation maps and ground truth masks, we consider the two as jointly distributed random variables and use the Pearson correlation between them. This metric is obtained by down sampling the masks to a lower resolution (e.g., 14×14) to reduce noise errors. Then we flatten the 2D masks into a 1D vectors and compute the correlation as:

$$\rho = \frac{\mathrm{cov}(X,Y)}{\sigma_X \sigma_Y} \tag{2}$$

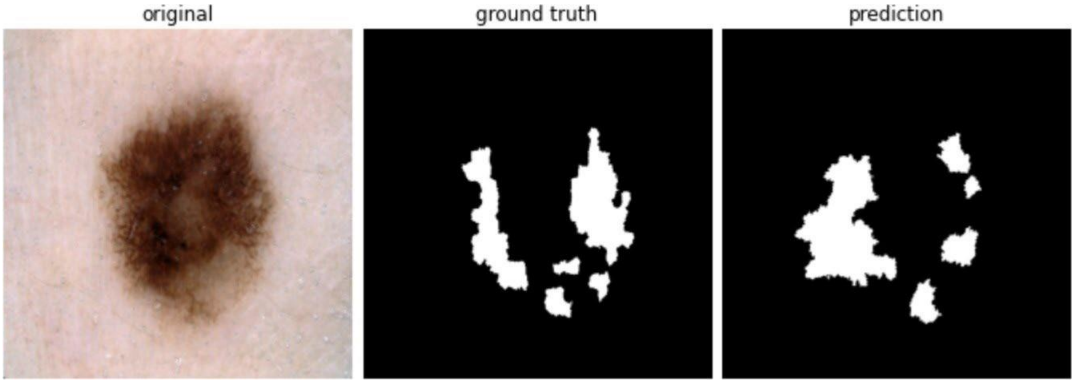

Figure 3. Left: Example of an image used to evaluate ensembles of explanations Middle: Ground-truth masks for an image in the ISIC-2018 melanoma dataset. Right: Explanation generated by averaging explanations generated by an ensemble of models.

3. **Center of Mass Distance** We compute the center of mass of a saliency or heatmap identified by the XAI algorithm. The center of mass R is computed as a function of each weight w at point r.

$$R = \frac{1}{W}\sum_{i=1}^{n} w_i r_i \quad \text{where} \quad W = \sum_{i=1}^{n} w_i \qquad (3)$$

Figure 3 illustrates the center of mass identified by ten networks for the wingbar of a bird. The black arrows indicate the center of mass of the heatmap of individual networks, and the red arrow indicates the center of mass of the ensemble explanation.

We compute the Euclidean distance from the center of mass to the key point identified by human annotator. The distance between the center of mass and a key point is useful for two reasons. First, it is quicker to collect key points vs. regions, i.e., pointing to a bird’s bill vs. tracing it. Second, many explanations in medical journals or bird watching guides use arrows instead of heatmaps to identify features, and the center of mass can be used as the endpoint of the arrowhead.

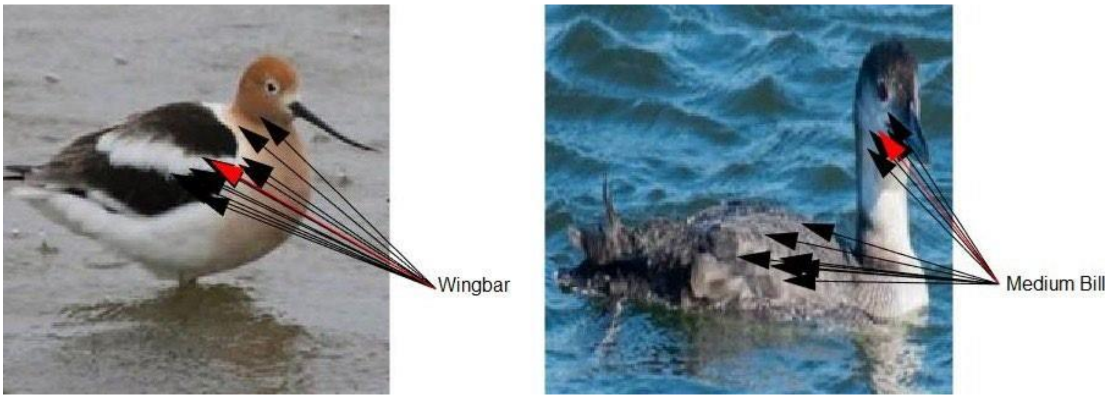

Figure 4. Use of key points that show center of mass (CoM) for heatmaps. The red arrowhead points to the CoM of the average heatmap while black arrows point to the CoM by each model inthe ensemble.

3.3. XAI Methods

We evaluated the averaging approach on multiple XAI methods to show the generality of the approach. The methods that we explored are surveyed in [5] and include, GradCAM and Guided GradCAM [26], LIME [23], Input gradient [27], Gradient SHAP [19], Integrated Gradients [31], and Saliency [28].

4. DATASETS

We train and evaluate our averaging algorithm on two datasets. Note that a dataset for evaluation must include ground truth labels and ground truth regions or key points. The regions or key points are used in evaluation, but not in training.

HiRes Birds HiRes Birds is a new dataset we introduce of 14,380 images of birds divided into 66 species. Additionally, we have collected data on various attributes of each bird, such as its bill length, wing pattern and location of the bill. We continue to collect additional feature and location information for this dataset. In this paper, we use this dataset to learn to identify attributes of the bird, such as whether it has a striped wing and evaluate whether the XAI algorithm focuses on the wing when making this classification.

ISIC-2018 ISIC-2018[7] is a melanoma detection dataset consisting of skin lesions obtained from a variety of anatomic sites and patients spread out across multiple different institutions. It consists of 2594 images along with 5 segmentation masks per image to identify the location of attributes of the region such as streaks and milia-like cysts. We only use the segmentation masks in evaluation. We train networks to recognize the presence or absence of features such as “milia-like cysts” and evaluate whether XAI algorithms find the region identified by the segmentation masks.

5. RESULTS

In this section, we first present data that shows averaging explanations from an ensemble of learners improves the explanation for a variety of XAI algorithms using initial random weights to create the ensemble. Next, we show results that vary the conditions under which the ensemble is learned to go deeper into the conditions under which the approach is effective. To assess the performance of our proposed method, we define two quantities: Individual Average (Ind-Avg) and Ensemble Average (Ens-Avg). Individual Average is the average metric on the evaluation set of each of the individual networks in the ensemble in the case that the ensemble is trained with random weights, or the individual network trained on all the training data in the case of bagging and leave-out-one-fold. Ensemble Average calculates an average heatmap and we report the target metric between the average heatmap and the ground truth.

5.1. HiRes Birds Results

We consider two different classification tasks with the HiRes Birds dataset. In both cases, we create ensembles starting with different random weights.

First, we train on a multi-class problem of identifying the bill length of the birds. For this task, there are 3 classes: Large, Medium and Small. We train on 4763 examples from the dataset using 530 as a validation set and 2322 as an evaluation set. We used Hive Data (a crowd-sourcing platform for data labelling) to collect both the bill length data and the bill location data. Our dataset includes a key point for each bill.

Table 1 shows the distance between the center of mass of the region found by 5 XAI algorithms using VGG16 as the deep learning classifier. Table 2 shows the data using ResNet as the deep learning classifier. In these tables, statistically significant results using a paired t-test are shown in bold with p-value < 0.01 indicated by ** and p-value < 0.0001 indicated by ****. The results show that for five commonly used XAI algorithms and two commonly used deep learning architectures, our ensemble method results in better identification of the center of mass that can be compared to a key point.

In our second use of HiRes Birds, we train on a multi-class problem of distinguishing the wing pattern of birds. For this task, there are 6 classes. We train on 12221 examples from the dataset using 2156 as a validation set. We have collected wing patterns for our data, but not the wing location. Therefore, we evaluate on the location of the wing using the bird data from the PartImageNet which contains wing locations but not patterns. The evaluation is based on the ground truth locations of wings in 594 bird images from the PartImageNet dataset.

Table 1. Ensembling improves explanation center of mass distance on the beak size identification task with VGG16 [29]. Ind-Avg refers to average performance of individual models evaluated separately. Ens-Avg refers to performance of the ensemble model. Lower is better. Best results are in bold

Table 1. Ensembling improves explanation center of mass distance on the beak size identification task with VGG16 [29].

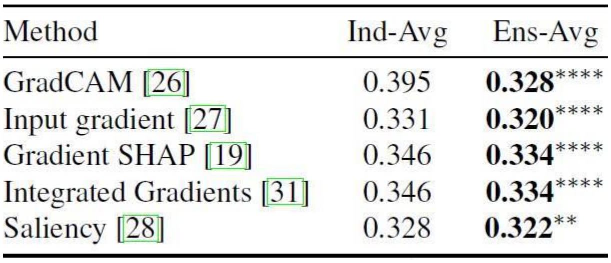

Method	Ind-Avg	Ens-Avg
GradCAM [26]	0.395	**0.328******
Input gradient [27]	0.331	**0.320******
Gradient SHAP [19]	0.346	**0.334******
Integrated Gradients [31]	0.346	**0.334******
Saliency [28]	0.328	**0.322****

Table 2. Ensembling improves explanation center of mass distance on the beak size identificationtask with ResNet18.

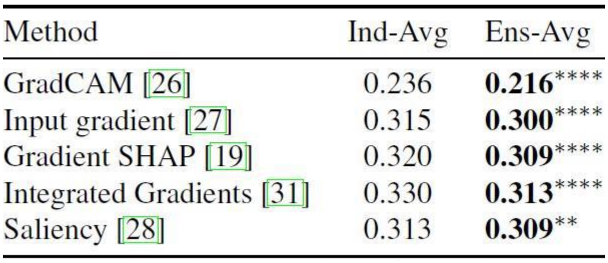

Method	Ind-Avg	Ens-Avg
GradCAM [26]	0.236	**0.216******
Input gradient [27]	0.315	**0.300******
Gradient SHAP [19]	0.320	**0.309******
Integrated Gradients [31]	0.330	**0.313******
Saliency [28]	0.313	**0.309****

Table 3 shows the correlation between the importance of pixels identified by XAI algorithms and the wing region in PartImageNet using VGG16. As before, averaging over an ensemble improves the XAI algorithms we tested. In addition, we computed the center of the PartImageNet wing regions and compared to the center of mass of the regions found by various XAI algorithms. The results shown in Table 4 indicate improvement for this metric as well.

Table 3. Ensembling improves explanation correlation on the wing pattern identification task with ResNet18.

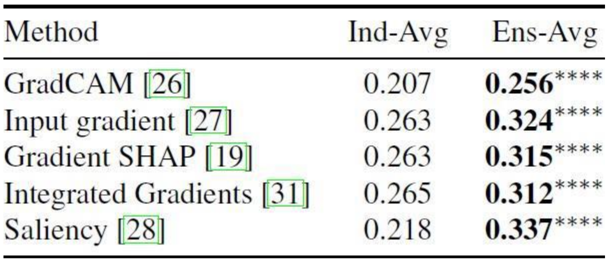

Method	Ind-Avg	Ens-Avg
GradCAM [26]	0.207	**0.256******
Input gradient [27]	0.263	**0.324******
Gradient SHAP [19]	0.263	**0.315******
Integrated Gradients [31]	0.265	**0.312******
Saliency [28]	0.218	**0.337******

Table 4. Ensembling improves explanation center of mass distance on the wing pattern identification task with ResNet18.

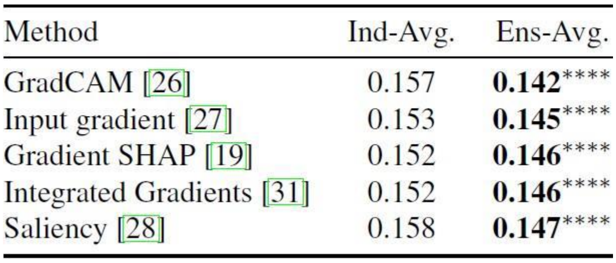

Method	Ind-Avg.	Ens-Avg.
GradCAM [26]	0.157	**0.142******
Input gradient [27]	0.153	**0.145******
Gradient SHAP [19]	0.152	**0.146******
Integrated Gradients [31]	0.152	**0.146******
Saliency [28]	0.158	**0.147******

5.2. ISIC-2018 Results

We also tested our method on the ISIC2018 dataset for melanoma lesion detection. For this task, each training image is paired with 5 dermatologist annotated masks that identify important attributes for melanoma detection. We train a five different multi-label binary classifier starting with random weights to output a binary variable for each of the 5 attributes of an image. We generate the ground-truth binary labels for an image by checking whether the associated ground-truth mask is non-zero or not. Once trained, we run different XAI algorithms to generate regions for each attribute that we compare to the segmentation mask in the evaluating data. We evaluate the quality of the generated explanations of individual models against our proposed method which averages the explanation across the ensemble. Results are reported in Table 5. We observe that for GradCAM and LIME we see a noticeable and statistically significant increase in explanation quality with ensemble explanations. Integrated-gradients and Saliency show small but nonetheless statistically significant improvements. We believe this is because Integrated-gradients and Saliency generate pixel level explanations whereas GradCAM and LIME generate region-based explanations leading to better IoU scores when comparing regions to segmentation masks.

Table 5. IoU between the ground truth and explanations generated from XAI methods on ISIC2018 dataset for the task of lesion identification.

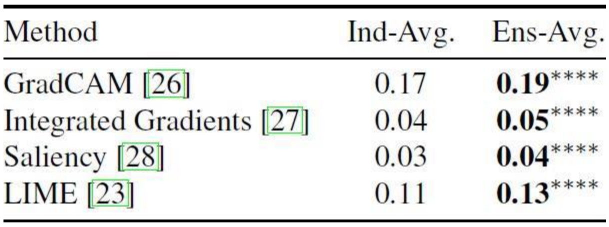

Method	Ind-Avg.	Ens-Avg.
GradCAM [26]	0.17	**0.19******
Integrated Gradients [27]	0.04	**0.05******
Saliency [28]	0.03	**0.04******
LIME [23]	0.11	**0.13******

Our trained classifiers achieve a mean Area under the ROC curve (AUC) score of 0.82 on the validation set. Ensembling the models leads to an improved AUC score of 0.86, showing that in addition to increasing explanation accuracy, classification accuracy is also increased. The increase in accuracy is statistically significant with a p-value of 0.03.

5.3. Separating the Effect on Intersection and Union

Here, we investigate the effect of averaging explanations on the intersection and union metrics independently using the same training procedure described in section 5.2. A greater intersection means that the XAI algorithm finds more of the area of interest identified by an annotator. A smaller union indicates that fewer regions are found outside the relevant region. Both intersection and union are measured in pixels.

Table 6 shows that the average explanation increases the intersection and decreases the union for LIME, integrated gradients, and saliency. This indicates that averaging finds more relevant regions and fewer irrelevant regions. For GradCAM, both the intersection and union increase but the increase in the intersection is more significant, leading to an overall improvement in the IoU score.

Table 6. Intersection (I) and Union (U) metrics for melanoma dataset. Ind-Avg is the average ofthe metric of individual models. Ens-Avg is the metric for our proposed technique. The unit of measurement for both intersection and union is pixels.

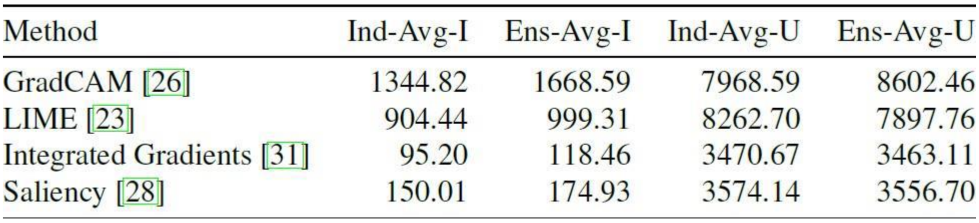

Method	Ind-Avg-I	Ens-Avg-I	Ind-Avg-U	Ens-Avg-U
GradCAM [26]	1344.82	1668.59	7968.59	8602.46
LIME [23]	904.44	999.31	8262.70	7897.76
Integrated Gradients [31]	95.20	118.46	3470.67	3463.11
Saliency [28]	150.01	174.93	3574.14	3556.70

5.4. Other Approaches to Creating an Ensemble

We also tried training an ensemble on the HiRes Birds beaks dataset using the Leave-Out-One method of creating an ensemble. In this setting, we divide the training data into K = 10 folds and then train each model in an ensemble of size 10 with a unique combination of 9 folds. In a similar experiment, we trained another ensemble of size 10 using a bagging algorithm where the training set for each model is generated by sampling from the original training set with replacement. The results for both experiments are reported in Table 7. We observe that both K-fold and bagging lead to improved explanation accuracy when compared to explanations generated by individual models trained on the entire training data.

Table 7. Center of mass distance between explanations and ground-truth annotations for an ensemble trained using the K-fold and Bagging algorithms. Ind-Avg is the CoM distance of asingle model trained on the entire training data. Lower is better.

Method	Ind-Avg	K-fold	Bagging
Guided GradCAM [26]	0.169	**0.153****	0.157
GradCAM[26]	0.297	**0.273****	0.277
Integrated Gradients [31]	0.278	**0.217****	0.219
Saliency [28]	0.280	**0.222****	0.225
Input gradient [27]	0.293	**0.241****	0.243
Gradient SHAP[19]	0.278	**0.218****	0.219

The results show that other ways of creating diverse models also works with our ensemble averaging method.

5.5. Varying the Size of the Ensemble

Next, we investigated the effect of ensemble size on the quality of the averaged explanation using the melanoma dataset. Fig. 5 plots the IoU score of the averaged explanation and the average IoU score of individual models against the size of the ensemble using the random weights method. We observe that IoU scores tend to increase with ensemble size and plateau after a certain threshold.

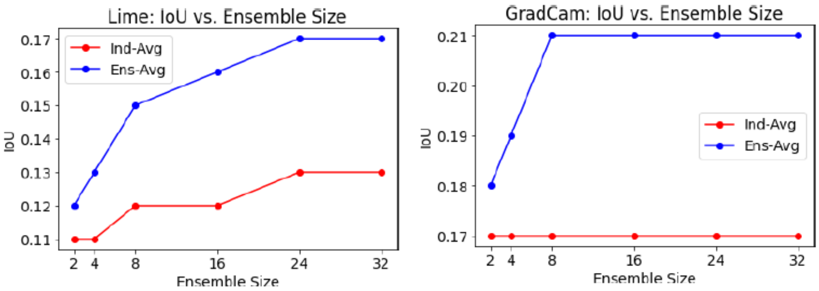

Figure 5. IoU between ground truth and generated explanations on ISIC-2018 dataset as a function of ensemble size. The blue curve shows the IoU score from our proposed technique which averages the explanations across the ensemble. The red curve shows the average of the individual IoU scores in the ensemble.

6. HUMAN EVALUATION

In this section, we show that people can notice the difference in the quality of explanations produced by ensembles when compared to individual models. In our computational experiments, the ensemble results in greater identification of regions of interest and less identification of irrelevant regions. The stimuli for the experiment consisted of images annotated by LIME or averaging of an ensemble of eleven LIME classifiers starting with different random weights. The stimuli were generated using the version of imageLIME in MATLAB. Figure 6 shows examples of the stimuli used in the experiment.

In Figure 6, the top bird is a common goldeneye. Its distinguishing characteristics (called field marks by birders) include a gold-colored eye, and it is distinguished from the similar Barrow's goldeneye by having a round vs. kidney-shaped patch on the cheek and striped vs. checkered wings. The averaged annotation on the right picks up both distinguishing characteristics, showing that averaging finds more relevant features. The middle bird is the Barrow’s Goldeneye and again the ensemble focuses on both the wing pattern and the cheek patch. The lower bird is a western grebe. It is distinguished from the similar Clark’s grebe by having a yellow vs. orange bill and having the black on the head extend below the eye. The average annotation on the right picks up both and furthermore does not emphasize a patch on the back that is not relevant to the classifications.

6.1. Participant Recruitment

This study was approved by UCSD’s IRB. Participants for this study were expert bird watchers who were recruited from mailing lists that report rare bird sightings in Southern California. We recruited 28 participants for a LIME vs. averaged LIME study: one participant self-excluded due to a lack of familiarity with the bird species included in the studies and did not complete the study, and one was excluded due to being under the age of 18, which may point to less real-world bird watching experience. In total, 26 participants were included in the analyses. Participants in the study had a median of 15 years of bird-watching experience.

6.2. Study Design

Prior to beginning the study, participants were shown an example of LIME used on an image of a dog to identify the features most important to classifying its breed. This example was intended to familiarize participants with how to interpret the colors on a LIME-generated heatmap. Each study contained 24 unique bird images, each of which was shown once to each subject with LIME-generated annotations and another time with averaged LIME-generated annotations. This results in 48 trials evenly split between the base LIME method and the averaged LIME method.

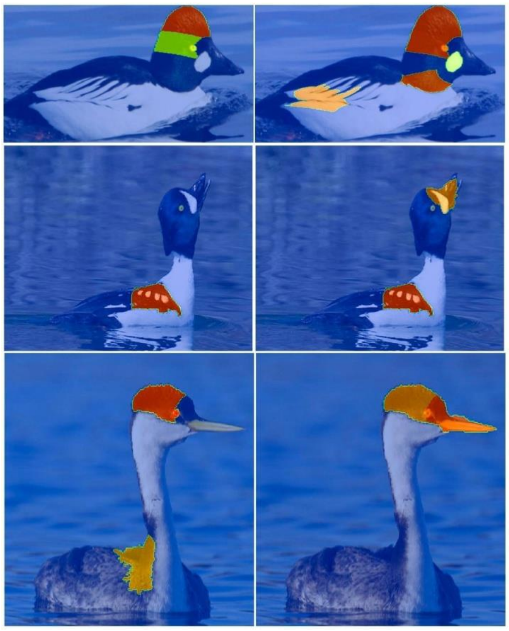

Figure 6. The figures on the left were annotated by LIME on a single VGG16 network. Theannotations of the figures on the right are the average of 11 VGG16 networks.

In addition, these 24 unique bird images consisted of 10 different bird species, and these ten bird species were selected to include five pairs of similar-looking birds:

- Black-headed grosbeak and blue grosbeak.
- Clark’s grebe and Western grebe.
- Eastern towhee and spotted towhee.
- Indigo bunting and lazuli bunting.
- The Barrow’s goldeneye and common goldeneye.

6.3. Results of Study

Each trial displayed heatmap-annotated bird images alongside unannotated images, a bird species classification task, and questions about annotation preferences. A screen capture of the study interface is shown in Figure 7. Participants were asked to classify the bird species in the image by selecting 1 of 10 radio buttons corresponding to the ten unique bird species. In each study, participants were asked to provide their opinions on the novel highlighting method by answering two questions: “This highlighting emphasizes the areas of the bird that I think are important for identification” (Question 1), and “I would recommend using this highlighting to identify this bird” (Question 2). Participants indicated their responses using a 7-point Likert scale ranging from “Strongly Agree” (a value of 7) to “Strongly Disagree” (a value of 1). The midpoint (a value of 4) indicates a “Neutral” sentiment.

We compared the median preference ratings for LIME trials to averaged LIME trials. We only include trials in which the subject correctly identified the bird species in calculating median preference ratings. The median classification accuracy across all participants was greater than 90%. Thus, participants were generally very accurate in their bird species classification, resulting in excluding a few trials per participant.

Bird images annotated by averaged LIME were preferred over annotations from LIME by a significant margin for both questions (p-value < 0.001 for both Question 1 and Question 2). All reported p-values are Bonferroni-corrected for 3 pairwise Mann–Whitney U tests. Broadly, subjects exhibit a significant preference for averaged LIME over standard LIME. Question 1 was given a median rating of 4.0 (“Neutral”) for LIME images. This increased to 5.5 (“Slightly Agree”/“Agree”) for averaged LIME images. Question 2 was given a median rating of 3.0 (“Slightly Disagree”) for LIME images. Averaging over an ensemble increased this to (“Slightly Agree”).

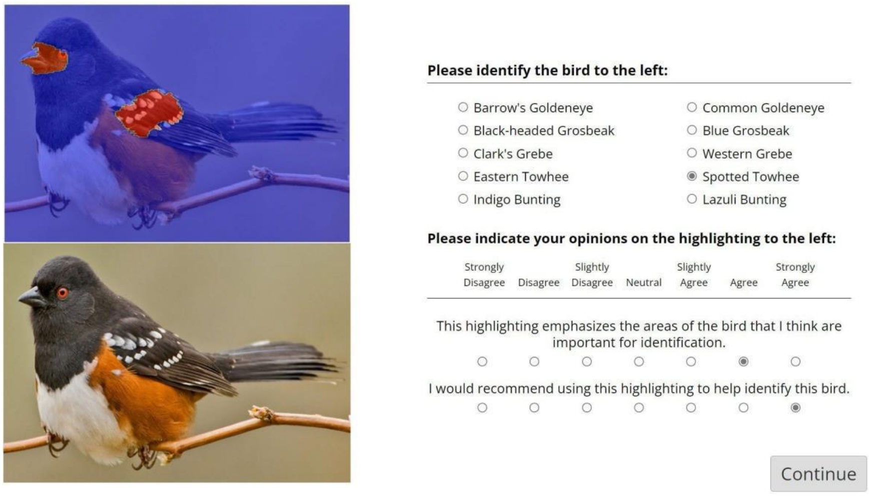

Please identify the bird to the left:

○ Barrow's Goldeneye	○ Common Goldeneye
○ Black-headed Grosbeak	○ Blue Grosbeak
○ Clark's Grebe	○ Western Grebe
○ Eastern Towhee	● Spotted Towhee
○ Indigo Bunting	○ Lazuli Bunting

Please indicate your opinions on the highlighting to the left:

	Strongly Disagree	Disagree	Slightly Disagree	Neutral	Slightly Agree	Agree	Strongly Agree
This highlighting emphasizes the areas of the bird that I think are important for identification.	○	○	○	○	○	●	○
I would recommend using this highlighting to help identify this bird.	○	○	○	○	○	○	●

Figure 7. An example screen capture from the study.

An alternative method of analyzing the responses keeps all trials, including those in which the subject incorrectly identified the bird’s species. This may be reasonable since the birder may know for example that the coloring around the eye is important for distinguishing grebes, but not recall whether the Western or Clark’s grebe has black below the eye. Including all trials, even those with incorrect classifications do not significantly differ in the distribution of preference ratings for any question for any highlighting method; averaged LIME remains significantly preferred over regular LIME for both questions at least with p-value < 0.001.

Subjects in general thought the ensembles led to improved highlighting areas that are important for identification and would recommend using that over the regions identified by a single model.

7. Future Work

We have shown that a simple average of networks increases the accuracy of explanations. However, in ensemble learning for classification accuracy, more complex methods such as boosting [12] have been developed. Boosting generates models that focus on correcting errors of other ensemble members and differentially weights the contributions of different ensemble members. This leads us to consider alternative combination algorithms.

One challenge is that boosting requires a ground truth classification, while we do not use ground truth explanations in training. A possible approach is to adopt methods in which weights are a function of correlations between classifications [1] to the situation where there are correlations across explanations.

Our user-study used LIME as the XAI algorithm. Our future work will explore other XAI algorithms. Our ultimate goal is to develop and evaluate with end users a new method that produces explanations similar to the expert explanation in Figure 2b with labeled regions. To achieve this, we need to accurately identify the regions, and the ensemble technique in this paper is an important step toward this goal.

8. Conclusion

XAI algorithms were developed to increase trust in deep learning algorithms for tasks such as image classification. However, XAI algorithms themselves need to be trustworthy. It has been shown that differences in training and initial conditions can produce different explanations and that the explanations of current XAI systems fail to identify all regions of importance used by human experts.

In this paper, inspired by the success of ensembles to increase classification accuracy, we proposed using ensembles to improve the explanation accuracy of saliency-based XAI algorithms. We show, through empirical results, that ensembles can improve the accuracy of explanations when measured using metrics such as IoU, correlation, and center of mass distance. Furthermore, we showed that explanations produced by ensembles are preferred by people over explanations produced bya single network. By looking for areas of consensus across multiple networks, ensembles reduce the irrelevant areas and increase the relevant areasin explanation.

Acknowledgements

This work was supported with funding from the DARPA Explainable AI Program under a contract from NRL and from NSF grant 2026809. We would like to thank Dave Gunning for stimulating XAI research. Discussions with David Aha, Albert Hsiao, and Justin Huynh were helpful in developing the ideas in this paper.

REFERENCES

[1] K. M. Ali and M. J. Pazzani, “Error reduction through learning multiple descriptions,” Machine learning, vol. 24, no. 3, pp. 173–202, 1996.

[2] N. Arun, N. Gaw, P. Singh, K. Chang, M. Aggarwal, B. Chen, K. Hoebel, S. Gupta, J. Patel, M. Gidwani et al., “Assessing the trustworthiness of saliency maps for localizing abnormalities in medical imaging,” Radiology: Artificial Intelligence, vol. 3, no. 6, p. e200267, 2021.

[3] P. P. Brahma, D. Wu, and Y. She, “Why deep learning works: A manifold disentanglement perspective,” IEEE Transactions on Neural Networks and Learning Systems, vol. 27, no. 10, pp. 1997–2008, 2016.

[4] L. Breiman, “Bagging predictors,” Machine learning, vol. 24, no. 2, pp. 123–140, 1996.

[5] S. Chakraborty et al., “Interpretability of deep learning models: A survey of results,” in 2017 IEEE smartworld, ubiquitous intelligence & computing, advanced & trusted computed, scalable computing & communications, cloud & big data computing, Internet of people and smart city innovation (smartworld/SCALCOM/UIC/ATC/CBDcom/IOP/SCI). IEEE, 2017, pp. 1–6.

[6] S. Chakraborty, R. Tomsett, R. Raghavendra, D. Harborne, M. Alzantot, F. Cerutti, M. Srivastava, A. Preece,

S. Julier, R. M. Rao et al., “Interpretability of deep learning models: A survey of results,” in 2017 IEEE smartworld, ubiquitous intelligence & computing, advanced & trusted computed, scalable computing & communications, cloud & big data computing, Internet of people and smart city innovation (smartworld/SCALCOM/UIC/ATC/CBDcom/IOP/SCI). IEEE, 2017, pp. 1–6.

[7] N. C. F. Codella et al., “Skin lesion analysis toward melanoma detection 2018: A challenge hosted by the international skin imaging collaboration (ISIC),” CoRR, vol. abs/1902.03368, 2019. [Online]. Available: http://arxiv.org/abs/1902.03368

[8] L. A. de Souza Jr, R. Mendel, S. Strasser, A. Ebigbo, A. Probst, H. Messmann, J. P. Papa, and C. Palm, “Convolutional neural networks for the evaluation of cancer in barrett’s esophagus: Explainable ai to lighten up the black-box,” Computers in Biology and Medicine, vol. 135, p. 104578, 2021.

[9] T. G. Dietterich, “Ensemble methods in machine learning,” in International workshop on multiple classifier systems. Springer, 2000, pp. 1–15.

[10] P. Domingos, “A unified bias-variance decomposition,” in Proceedings of 17th International Conference on Machine Learning, 2000, pp. 231–238.

[11] X. Dong, Z. Yu, W. Cao, Y. Shi, and Q. Ma, “A survey on ensemble learning,” Frontiers of Computer Science, vol. 14, no. 2, pp. 241–258, 2020.

[12] Y. Freund, R. E. Schapire et al., “Experiments with a new boosting algorithm,” in icml, vol. 96. Citeseer, 1996, pp. 148–156.

[13] M. Gams, “New measurements highlight the importance of redundant knowledge,” in Proceedings of the 4th European Working Session on Learning (EWSL89), 1989, pp. 71–80.

[14] K. He, X. Zhang, S. Ren, and J. Sun, “Deep residual learning for image recognition,” in Proceedings of the IEEE conference on computer vision and pattern recognition, 2016, pp. 770–778.

[15] A. Krizhevsky, I. Sutskever, and G. E. Hinton, “Imagenet classification with deep convolutional neural networks,” Advances in neural information processing systems, vol. 25, 2012.

[16] S. Lapuschkin, A. Binder, G. Montavon, K.-R. Mu¨ller, and W. Samek, “The lrp toolbox for artificial neural networks,” The Journal of Machine Learning Research, vol. 17, no. 1, pp. 3938–3942, 2016.

[17] Y. LeCun, Y. Bengio, and G. Hinton, “Deep learning,” nature, vol. 521, no. 7553, pp. 436–444, 2015.

[18] Y. Liu and X. Yao, “Ensemble learning via negative correlation,” Neural networks, vol. 12, no. 10, pp. 1399– 1404,1999.

[19] S. M. Lundberg and S.-I. Lee, “A unified approach to interpreting model predictions,” Advances in neural information processing systems, vol. 30, 2017.

[20] S. M. Lundberg and S. Lee, “A unified approach to interpreting model predictions,” CoRR, vol. abs/1705.07874, 2017. [Online]. Available: http://arxiv.org/abs/1705.07874

[21] Mar, V.J., Soyer, H., Button-Sloan, A., Fishburn, P., Gyorki, D.E., Hardy, M., Henderson, M. and Thompson, J.F., 2020. Diagnosis and management of cutaneous melanoma. Australian journal of general practice, 49(11), pp.733-739.

[22] M. Pazzani, R. K. Severine Soltani, S. Qian, and A. Hsiao, “Expert-informed, user-centric explanations for machine learning,” in Proceedings of the AAAI Conference on Artificial Intelligence-2022. IOS Press, 2022.

[23] M. T. Ribeiro, S. Singh, and C. Guestrin, “” why should i trust you?” explaining the predictions of

any classifier," in Proceedings of the 22nd ACM SIGKDD international conference on knowledge discovery and data mining, 2016, pp. 1135–1144.

[24] L. Rieger and L. K. Hansen, "Aggregating explainability methods for neural networks stabilizes explanations," arXiv preprint arXiv:1903.00519, 2019.

[25] W. Samek, A. Binder, G. Montavon, S. Lapuschkin, and K.-R. Mu¨ller, "Evaluating the visualization of what a deep neural network has learned," IEEE transactions on neural networks and learning systems, vol. 28, no. 11, pp. 2660–2673, 2016.

[26] R. R. Selvaraju, M. Cogswell, A. Das, R. Vedantam, D. Parikh, and D. Batra, "Grad-cam: Visual explanations from deep networks via gradient-based localization," in Proceedings of the IEEE international conference on computer vision, 2017, pp. 618–626.

[27] A. Shrikumar, P. Greenside, A. Shcherbina, and A. Kundaje, "Not just a black box: Learning important features through propagating activation differences," arXiv preprint arXiv:1605.01713, 2016.

[28] K. Simonyan, A. Vedaldi, and A. Zisserman, "Deep inside convolutional networks: Visualising image classification models and saliency maps," arXiv preprint arXiv:1312.6034, 2013.

[29] K. Simonyan and A. Zisserman, "Very deep convolutional networks for large-scale image recognition," arXiv preprint arXiv:1409.1556, 2014.

[30] A. Singh, S. Sengupta, A. R. Mohammed, I. Faruq, V. Jayakumar, J. Zelek, V. Lakshminarayanan et al., "What is the optimal attribution method for explainable ophthalmic disease classification?" in International Workshop on Ophthalmic Medical Image Analysis. Springer, 2020, pp. 21–31.

[31] M. Sundararajan, A. Taly, and Q. Yan, "Axiomatic attribution for deep networks," in International conference on machine learning. PMLR, 2017, pp. 3319–3328.

[32] M. Watson, B. A. S. Hasan, and N. Al Moubayed, "Agree to disagree: When deep learning models with identical architectures produce distinct explanations," in Proceedings of the IEEE/CVF Winter Conference on Applications of Computer Vision, 2022, pp. 875–884.

[33] X. L. Weina Jin and G. Hamarneh, "Evaluating explainable ai on a multi-modal medical imaging task: Can existing algorithms fulfill clinical requirements?" in Proceedings of the AAAI Conference on Artificial Intelligence-2022. IOS Press, 2022.

AUTHORS

Aadil Ahamed received his M.S. in Computer Science, Specialization in Artificial Intelligence from University of California, San Diego and his B.S. in Computer Engineering from University of California, Irvine.

Kamran Alipour received his PhD in Computer Science from University of California, San Diego in 2022 and M.S. in Aerospace Engineering from Sharif University of Technology and a B.S. in Aerospace from K. N. Toosi University of Technology

Sateesh Kumar is a Master's student at the Computer Science and Engineering department of UC San Diego. He obtained his bachelor's in Computer Science from National University of Computer and Emerging Sciences, Pakistan.

Severine Soltani completed her B.S. in Cognitive Science with a focus on machine learning and neural computation at UC San Diego in 2020. She is currently a Bioinformatics and Systems Biology Ph.D. student at UC San Diego, examining the effects of environmental perturbations on physiological data via wearable devices.

Michael Pazzani received his Ph.D. in Computer Science from University of California, Los Angeles. He is director of the Artificial Intelligence Research for Health Center at the Information Sciences Institute in Marina Del Rey, CA, USA